Synthesis of highly near-infrared fluorescent graphene quantum dots (GQDs) using biomass-derived materials for *in vitro* cell imaging and metal ion detection

Sarah Reagen¹, Yingfen Wu¹, Xiao Liu¹, Rahul Shahni¹, Jacob Bogenschuetz², Xu Wu¹, Qianli R. Chu¹, Nuri Oncel², Jin Zhang³, Xiaodong Hou³, Colin Combs⁴, Antonio Vasquez¹, and Julia Xiaojun Zhao*¹

¹Department of Chemistry, University of North Dakota, Grand Forks, North Dakota 58202, USA

² Department of Physics and Astrophysics, University of North Dakota, Grand Forks, North Dakota 58202, USA

³Institute for Energy Studies, University of North Dakota, Grand Forks, North Dakota 58202, USA

⁴Department of Biomedical Sciences, University of North Dakota, Grand Forks, North Dakota 58202, USA

Abstract

Graphene quantum dots (GODs) are a subset of fluorescent nanomaterials that have peaked recent interest due to their photoluminescence properties, low toxicity and biocompatibility features for bioanalysis and bioimaging. However, it is still a challenge to prepare highly near-infrared (NIR) fluorescent GQDs using a facile pathway. In this study, NIR GQDs were synthesized from the biomass-derived organic molecule cis-cyclobutane-1,2-dicarboxylic acid via one-step pyrolysis. The resulting GQDs were then characterized by various analytical methods such as UV-Vis absorption spectroscopy, fluorescence spectroscopy, dynamic light scattering (DLS), high resolution transmission electron microscopy (HRTEM), Fourier transform infrared spectroscopy (FT-IR), X-ray diffraction (XRD), and Xray photoelectron spectroscopy (XPS). Moreover, the photostability and stability over a wide pH range were also investigated, which indicated the excellent stability of the prepared GQDs. Most importantly, two peaks were found in the fluorescence emission spectra of the GQDs, one of which was located in the NIR region of about 860 nm. Finally, the GQDs were applied for cell imaging with human breast cancer cell line, MCF-7, and cytotoxicity analysis with mouse macrophage cell line, RAW 246.7. The results clearly showed the GQDs enter the cells through endocytosis on the fluorescence images and were not toxic to cells up to a concentration of 200 µg/mL. Thus, the developed GQDs could be a potential effective fluorescent bioimaging agent. Finally, the GQDs depicted fluorescence quenching when treated with mercury metal ions, indicating that the GQDs could be used for mercury detection in biological samples as well.

1. Introduction

A wide range of fluorescent nanomaterials have been implemented into vast areas of research since the development of nanotechnology. These nanomaterials include quantum dots, metal nanoparticles, rare-earth metal doped nanoparticles, inorganic dye-doped silica nanoparticles, polymer-encapsulated organic nanoparticles, and carbon nanomaterials.¹⁻⁴ Previously, semiconducting quantum dots (QDs) were ideal fluorescent probes, but due to the fact that most of these QDs are composed of heavy metals such as cadmium, which can cause both biological and environmental hazards in large enough quantities, alternative materials such has graphene and carbon have been considered.^{5,6} The derivative material of graphene has several important properties from mechanical to thermal with recent developments that have shown an increase in research interest for graphene quantum dots (GQDs). The most favorable characteristics include low toxicity, chemical inertness, stability, and biocompatibility compared to traditional QDs.⁵⁻¹⁸ GQDs also present fluorescence properties, which allows GQDs to be used in the detection of both inorganic and organic materials such as metal ions, organic polymer molecules, and anions. 15 In particular, fluorescence itself has been a vital tool for the development of imaging techniques to visualize key details in living cells and animals without involving potentially harmful radioactivity or electron burning. 10 The combination of these factors has made GQDs a considerable candidate in applications that involve bioimaging and metal sensing, among other applications. 10,13 Additionally GQDs have potential advancements for in vivo and in vitro fluorescence imaging due to functionalized GQDs having the capability of interacting with biological systems. 9,19-21 However, the field of GQDs is still relatively new with a need of more extensive research in order to broaden the use for in vitro and in vivo bioimaging techniques, especially when the GQDs can behave as key biomarkers. 8,22,23 Furthermore, GQDs with near infrared (NIR) fluorescence are extremely rare and scarcely reported despite being highly desirable for biomedical imaging applications.²⁴ Although there have been recent reports of NIR containing GQDs²⁵ and carbon dots²⁶, there remains several undesirable traits during synthesis procedures such as the use of strong acids²⁷, element doping^{28,29}, lengthy reactions³⁰, and forms of graphene oxide³¹. Additionally, may synthesized GQDs with NIR fluorescence usually contain their peak in the lower NIR region^{24,32,33} (650-810 nm) or are dependent on larger GQD particle size³⁴. NIR fluorescent materials for bioimaging are sought after due to their deep tissue penetration, weak emission light scattering, and lower background which helps improve signal-to-noise ratios. 24,35,36 Having a carbon-based nanomaterial that emits fluorescence in the NIR region would provide not only the above listed imaging benefits but also reduced toxicity and easier cellular uptake and integration because of their chemical make-up and small particle size.

GQDs have two primary means of synthesis; top-down or bottom-up. 8.22,23,37,38 The top-down method breaks down carbon source material by several different methods to synthesize GQDs; including lithography, oxidation, microfluidization, electrochemical, solvothermal, and microwave-assisted hydrothermal.^{21,38} The bottom-up method combines smaller groups of benzene derivatives and carbonization from organic polymers to form larger quantities of GQDs using stepwise solution chemistry, oxidation, hydrothermal heating, and pyrolysis. 8,21,38 The top-down method tends to be more extensive than the bottom-up approach, although the latter is more precise yet complicated with many synthesis steps.³⁹ Typically, molecules containing polycyclic aromatic rings are used as reliable precursors to form high-quality GQDs via the bottom-up approach.³⁸⁻⁴¹ These precursors are traditionally produced from non-renewable sources such as coal and petroleum coke. The rapidly increasing world population and irreversible consumption of limited fossil resources have been motivating researchers to develop new materials using sustainable sources. Several reports have recently suggested that renewable, inexpensive, and readily available biomass waste, such as rice husk, 42 dead leaves⁴³, waste peels⁴⁴, or food waste⁴⁵, have the potential to emerge as an alternative feedstock to produce GODs. Meanwhile, efforts have been made to utilize biomass-derived chemicals as precursors, including citric acid⁴⁶ and Lglutamic acid.⁴⁷ However, there are still few examples of high-quality GQDs derived from biomass when compared to the non-renewable petrochemicals.⁴⁸ Therefore, developing reliable biomass-derived precursors for creating highquality GQDs instead of petrochemical-based precursors for suitable applications remains highly desirable.

Furfural, one of the most valued biobased chemicals, is derived from an array of agro-residues such as wheat bran, corncobs, sugar cane bagasse, and sawdust. ^{49,50} Furfural has been serving as a vital starting material to produce a wide range of specialty chemicals and renewable building blocks for designing new materials. ^{51,52} One such furfural derived building block is *cis-*3,4-di(furan-2-yl)cyclobutane-1,2-dicarboxylic acid (CBDA-2). ⁵³ This furfural derived building block has shown potential applications in developing 100% bio-based cyclobutane-containing polymers (CBPs) exhibiting desirable chemical and thermal properties, which are potentially important in industry. In this work, GQDs were synthesized by bottom-up pyrolysis of the biomass-derived diacid CBDA-2 in NH₄OH/water solution. The obtained GQDs were analyzed for fluorescence characteristics and chemically characterized by various analytical methods for *in vitro* imaging and metal ion detection applications. These analytical techniques include UV-Vis

absorption spectroscopy, fluorescence spectroscopy, dynamic light scattering (DLS) for size distribution and zeta potential analysis, Fourier transform infrared spectroscopy, high resolution transmission electron spectroscopy (HRTEM), X-ray photoelectron spectroscopy (XPS), and confocal microscopy. Lastly, the GQDs were subjected to several concentrations of multiple metal ions to determine their capability of detecting these ions.

2. Experimental

2.1. Materials

2-[4-(2-hydroxyethyl)piperazin-1-yl]ethanesulfonic acid (HEPES buffer, 99.5%), 3-(cyclhexylamino)-1-propanesulfonic acid (CAPS buffer, ≥99%), 2-(cyclohexylamino)ethanesulfonic acid (CHES buffer, ≥99%), maleic acid (≥99%), citric acid (≥99.5%), FeCl₃, Pb(Ac)₂·3H₂O, and CuSO₄ were purchased from Sigma-Aldrich (St. Louis, MO, USA). Ammonium hydroxide (99%) and fluorescein dye were both purchased from Fisher Scientific (Hampton, NH, USA). HgCl₂ was purchased from ACROS Organics (Fair Lawn, NJ, USA) and FeSO₄·7H₂O was purchased from Sargent-Welch VWR Scientific (Buffalo Grove, IL, USA). Dulbecco's Modified Eagle Medium was purchased from Life Technologies/Thermo Fisher Scientific (Waltham, MA, USA). Fetal bovine serum was purchased from Peak Serum (Wellington, CO, USA). Penicillin-strep was purchased from Sigma Aldrich/Millipore (St. Louis, MO).8-well Chambered Coverglass w/ non-removable wells and TO-PRO®-3 Stain were purchased from Thermo Fisher(Waltham, MA,USA). Fluoromount-G® mounting medium was purchased from SouthernBiotech (Birmingham, AL). CytoTox 96® Non-Radioactive Cytotoxicity Assay kit was purchased from Promega (Madison, WI, USA).

2.2. Sample solution preparation

The 20 mM HEPES buffer solutions of pH 1.0, 3.0, 5.0, 7.0, 9.0, and 11.0 were prepared with the pH being adjusted by the addition of NaOH and HCl. For investigating photostability, all the samples were sonication for 30 min before analysis. For the detection of metal ions, 100, 10, and 1.0 μM solutions of CuSO₄, FeCl₃, FeSO₄, Pb(Ac)₂, and HgCl₂ were prepared in water. Based on the GQDs response to mercury ions, an optimization experiment was designed to test four changing factors of pH, temperature, concentration of Hg²⁺ and concentration of GQDs. These four parameters were used to design a 2⁴ screening factorial design in order to identify important factors impacting fluorescence intensity and to better analyze optimal analysis conditions.

2.3. Instrumentation for the characterization of GQDs

A Perkin Elmer Lambda 1050 UV-250 UV/Vis/NIR spectrophotometer was used for the UV/Vis absorption measurements of the GQDs. The fluorescence spectra and photostability measurements were acquired by a Shimadzu RF-6000 spectrophotometer. NIR fluorescence was measured by a Jobin-Yvon-Horiba Fluorometer 3 Model (FL 3-11 spectrofluorometer). A Marlwen model of Nano-ZS Zetasizer was used to measure the zeta potential and size distribution of GQDs in HEPES buffer with different pH values. A JEOL Jem 2100 Electron Microscope was used to obtain high resolution transmission electron microscopy (HRTEM) images of the GQDs. A Thermo Fisher Scientific Nicolet iS5 Fourier transform infrared spectrometer (FT-IR) was utilized to obtain the IR spectra of CBDA-2 and the GQDs. X-ray diffraction (XRD) measurements were analyzed on a Rigaku SmartLab and X-ray photoelectron spectroscopy (XPS) analysis was conducted on a Perkin Elmer model PHI 40-700. An Olympus FV3000 Laser Scanning Confocal Microscope was used for the *in vitro* cell imaging of the GQDs. Two channels were used for the imaging; those being red (Fura-Red (Ca-free)) and green (Alexa 488). MCF-7 cells were cultured over night with 100 µL of 0.8 mg/mL GQDs and TOPRO-3 labeled nuclei. Bright-field images were also collected at the same time for clarification of cell growth and location on the coverslips. A ELX800 plate reader was used for the cell viability experiments. GQDs with gradient concentrations were incubated overnight and the cell viability assay was followed using the protocol of CytoTox 96® Non-Radioactive Cytotoxicity Assay kit.

2.4. Synthesis of GQDs

CBDA-2 was synthesized from furfural in two steps. 44 In the first step, a key intermediate - *trans*-3-(2-furyl)acrylic acid was constructed by Knoevenagel condensation between furfural and malonic acid and the subsequent decarboxylation. In the second step, 2.0 g crystalline *trans*-3-(2-furyl)acrylic acid was ground into a fine powder and suspended in 100 mL of hexane in an Erlenmeyer flask equipped with magnetic stirring. The continuously stirred suspension was subjected to UV radiation of eight 13-watts residential blacklight (Feit Electric BPESL15T/BLB compact fluorescent twist bulb) for 12 h. After completion of reaction, the slurry was filtered to give CBDA-2 as a white solid (1.9 g, 95%).

To prepare GQDs, CBDA-2 was dissolved in DI-water with a final concentration of 4.0 mg/mL before the pH was brought to 10.0 using NH₄OH. The solution was then autoclaved for 12 h at 200 °C. Furthermore, a Spectra/Por Dialysis Membrane BioTech CE Tubing of MWCO 100-500 Da was used for the dialysis of the GQDs for 12 h before

being centrifuged for 30 min. The final concentration of the GQDs was calculated to be 2.0 mg/mL, which was store in a fridge for future usage.

2.5. Quantum yield measurement

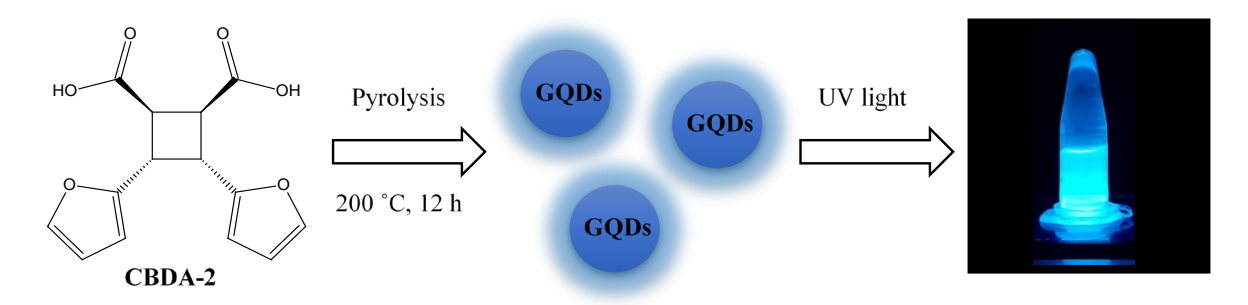
The quantum yield was calculated for the visible GQDs peak (440 nm) using Equation 1 below with quinine sulfate in 0.1 M H₂SO₄ as the standard reference.⁵⁴ Quinine sulfate in 0.1 M H₂SO₄ was previously determined to have a Φ_{st} of 0.54 with η_{st}^2 being equal to 1 in the case of 0.1 M H₂SO₄.⁵⁴ Similarly, the GQDs would also have η_x^2 equal to 1 when prepared in a pH 7.0 HEPES buffer. The quantum yield was calculated to be 45%.

$$\Phi_x = \Phi_{st} \left(\frac{Grad_x}{Grad_{st}} \right) \left(\frac{\eta_x^2}{\eta_{st}^2} \right)$$
 (Eq. 1)

3. Results and Discussions

3.1. Design of the synthesis of GQDs using biomass

The goal of this work was to develop a simple yet effect method for the synthesis of fluorescent graphene quantum dots that could be used in bioimaging applications as well as metal ion detection. Traditional bottom-up methods for GQDs synthesis utilize organic precursors, such as amino acids, citric acid, histidine, L-glutamic acid, and glucose.³⁸ Inspired by those starting materials and the low-cost properties of biomass materials, we developed a method for synthesizing GQDs using a biomass derived molecule from furfural, CBDA-2. CBDA-2 was obtained from biomass that was also non-toxic. Through the simple pyrolysis at 200 °C for 12 h, the fluorescent GQDs were synthesized. Under the irradiation of UV light, the prepared GQDs showed bright blue fluorescence (Scheme 1).



Schematic 1: CBDA-2 conversion to GQDs by pyrolysis under basic conditions. Exposure to UV light shows that the newly synthesized material contains fluorescent properties.

3.2. Characterization of the synthesized GQDs

To confirm the obtained nanomaterials of the GQDs designed, a number of characterization experiments were conducted. First, the morphology and size of the GQDs were characterized. To clearly observe the crystal structure of the GQDs, a high resolution transmission electron microscope (HRTEM) was employed. The results were shown in Figure 1. Both larger clusters (Figure 1A) and enlarged single particle GQDs (Figure 1B) were observed.

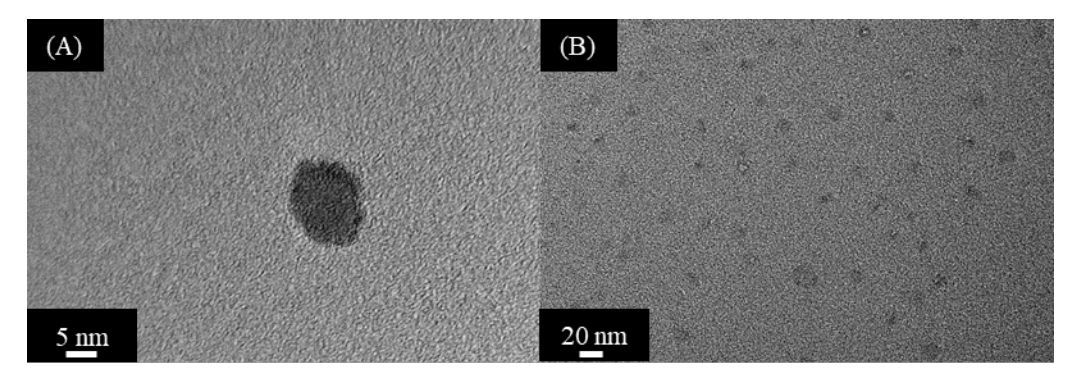


Figure 1: HRTEM images of the GQDs, 2.0 mg/mL. (A) individual particle that are $\sim 4-7 \text{ nm}$ in diameter; (B) image of particle dispersion that show no agglomeration.

The size distribution of the GQDs was statistically measured using DLS (Figure 2). To better observe the individual particles, the GQDs were sonicated for 30 min prior to analysis. The resulting table shows that the GQDs range from approximately 3-10 nm with an average size of 6.5 ± 3.5 nm. This is conclusive with the HRTEM images, which show individual particles around 4-7 nm, with a decent dispersion of the particles.

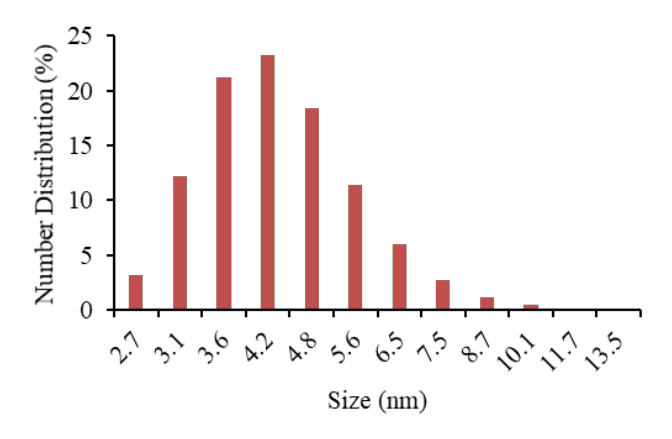


Figure 2: Size distribution of sonicated GQDs in water by DLS, $20 \mu g/mL$. Individual GQDs are approximately 3-10 nm.

The zeta potential of the GQDs in different pHs was also analyzed (Figure 3). The results showed that in the range of pH 7.0-11.0, GQDs had high zeta potentials of -35.6, -26.2, and -22.5 mV, respectively. Comparatively, pH 5.0 showed a moderate decrease of zeta potential at -9.7 mV. The remaining solutions of pH 3.0 and 1.0 show the lowest zeta potentials of approximately -2.2 and +7.3 mV, and therefore contain the highest agglomeration. Based on these results, the GQDs were more stable in basic pH solutions of 7.0-11.0 and stable moderately in pH 5.0.

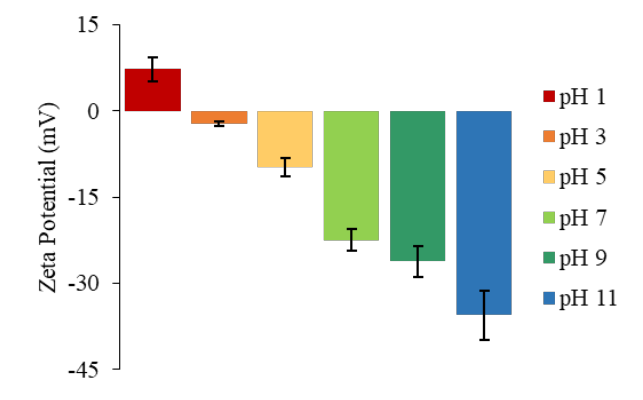


Figure 3: Zeta potential measurements of the GQDs in the maelate (pH 1), citrate (pH 3 and 5), HEPES (pH 7), CHES (pH 9) and CAPS (pH 11) buffers. All GQD solutions were in concentrations of 0.2 mg/mL.

Furthermore, the functional groups of the GQDs were investigated using FT-IR spectra (Figure 4). First, the starting material of CBDA-2 was measured (Figure 4, red). The spectrum of CBDA-2 showed two clear peaks at 3103 and 1697 cm⁻¹ that are attributed to -OH and C=O functional groups, respectively.^{55,56} In comparison, the GQDs contained four characteristic peaks at 3207, 2923, 1684, and 1559 cm⁻¹ (Figure 4, blue), which are labeled to the functional groups of -OH, sp^3 C-H, C=O, and C=C, respectively.⁵⁷⁻⁶¹ In comparison, the GQDs and CBDA-2 share some similar functionality in the forms of alcohol and carbonyl groups. However, the GQDs show additional peaks of the olefin type and additional sp^3 hybridized C-H bonds. This strongly indicating a reaction that charged the chemical structure of the GQDs from CBDA-2 that thus yields fluorescent properties.

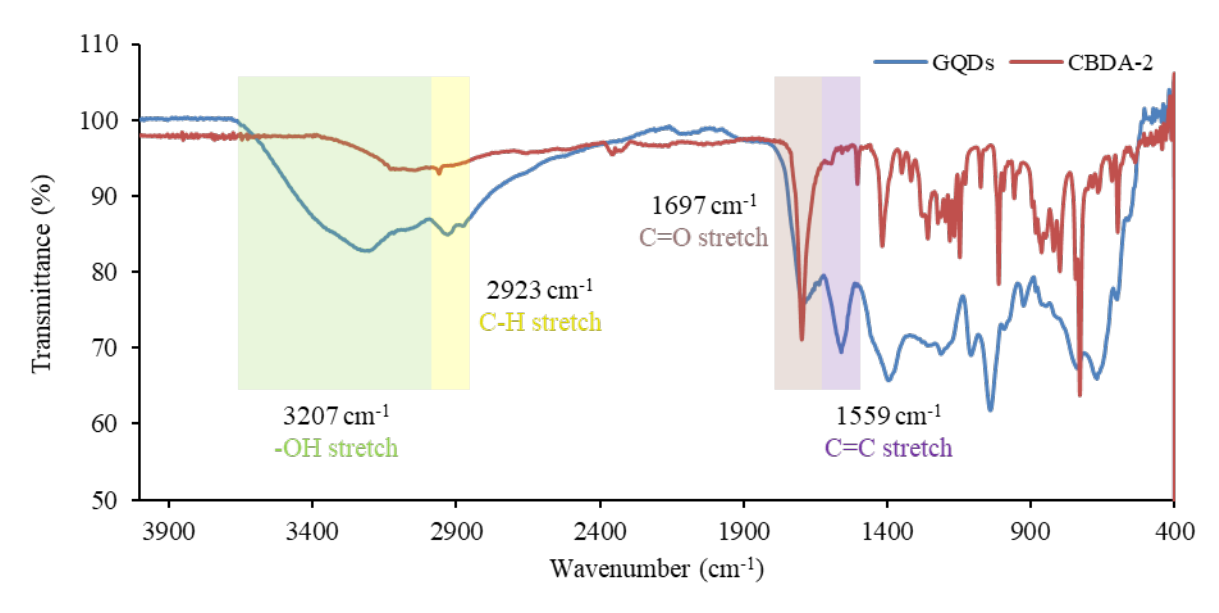


Figure 4: FT-IR spectra of CBDA-2 (red) and the GQDs (blue). The two compounds share similar peaks in the alcohol and carbonyl regions but differs with the GQDs having additional olefin and sp³ C-H peaks.

The composition of the GQDs was further analyzed using XRD and XPS techniques. As shown in Figure 5, the XPS analysis results suggested that the prepared GQDs are composed mainly of carbon and oxygen with two main peaks: oxygen (531 eV) and carbon (284 eV) (Figure 5A), which is in agreement with the literature. Also, two smaller peaks were seen in the range of 1020-970 eV, which is consistent with carbon as graphite. Additionally, it is of note that the oxygen peak has a left-field shift; typical oxygen peaks have a range of 528-534 eV while this oxygen peak has a range of approximately 529-538 eV. This is also consistent in the mica (blank) spectrum; thus, it was deduced that the functionality ranges within the oxygen peak were also shifted to the left. The carbon peak was not shifted for either the mica or the GQDs, and remains in the functionality ranges of the peak. Therefore, the shifted oxygen peak could have been a calibration issue with the instrument. High-resolution XPS of C 1s demonstrated three peaks at 286.7, 285.67, and 288.11 eV, which were attributed to C-O-C, C-C, and C=O, respectively (Figure 5B). The O 1s spectrum showed two major peaks at 531.14 and 533.05 eV for C=O and C-O, respectively (Figure 5C).

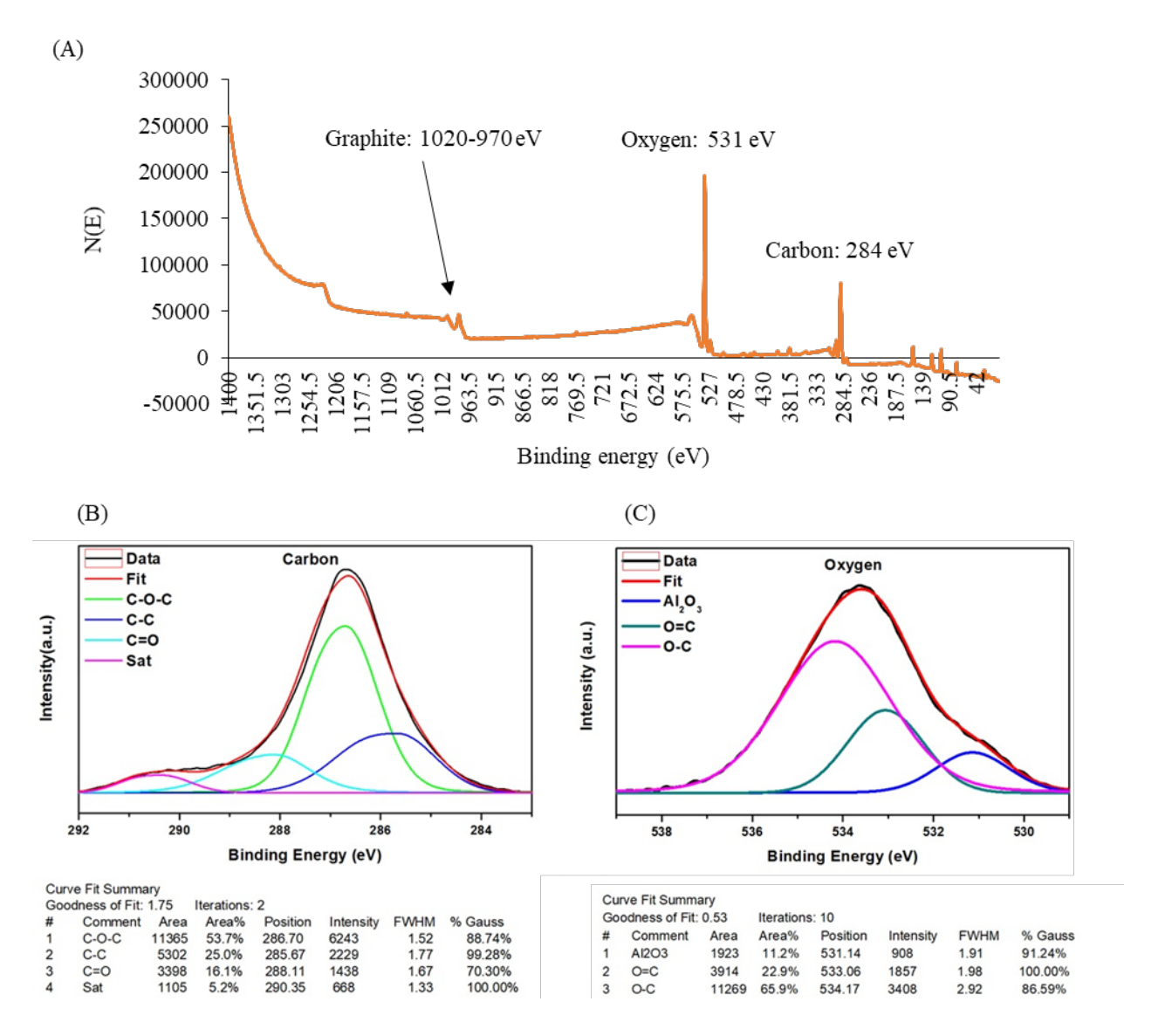


Figure 5: (A) Entire XPS spectrum of the GQDs shows the left-field shift of the oxygen peak at around 531 eV and the carbon peak at 284 eV. Graphite peaks are visible in the 1020-970 eV range. XPS graphs of the carbon (B) and oxygen (C) peaks of the GQDs (2 mg/mL). The carbon peak shows clear distribution of the functional groups within. The oxygen peak has regions of unknown groups, most likely due to the peak shift of the instrument.

Additionally, the XRD pattern (Figure 6) of the GQDs showed a broad peak centered at 20° (d spacing = 0.44 nm) that could be attributed to the π - π stacking of GQDs. Neither a characteristic (002) peak of graphene oxide at around 10° nor a sharp 0020 peak of graphene at 26.5° were observed, which implies the two-dimensional nature of the GQDs which lack a long distance order (i.e. a small thickness) along (002) direction (c-axis). These results were strongly consistent with the results of previous reports. $^{63-65}$

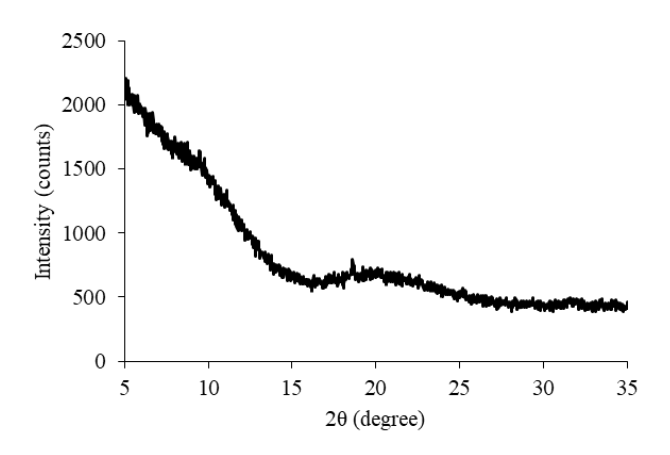


Figure 6: XRD analysis of the GQDs shows a distinctive peak at 20°, an indication of graphene within the sample.

3.3. Optical properties of the GQDs

The most important designed feature of the GQDs is their fluorescence properties. This property was investigate using both spectroscopy and microscopy. The UV-Vis absorption and fluorescence emission spectra of the GQDs were recorded in a 0.2 mg/mL aqueous solution. As shown in Figure 7A, the GQDs showed two UV-Vis adsorption peaks at about 230 and 300 nm, which were attributed to $\pi - \pi^*$ transition of the C-C bond and the n- π^* transition of the oxygen-containing groups. When the GQDs were excited with 310 nm radiation, the GQDs emitted a strong fluorescence peak at 440 nm (Figure 7B).

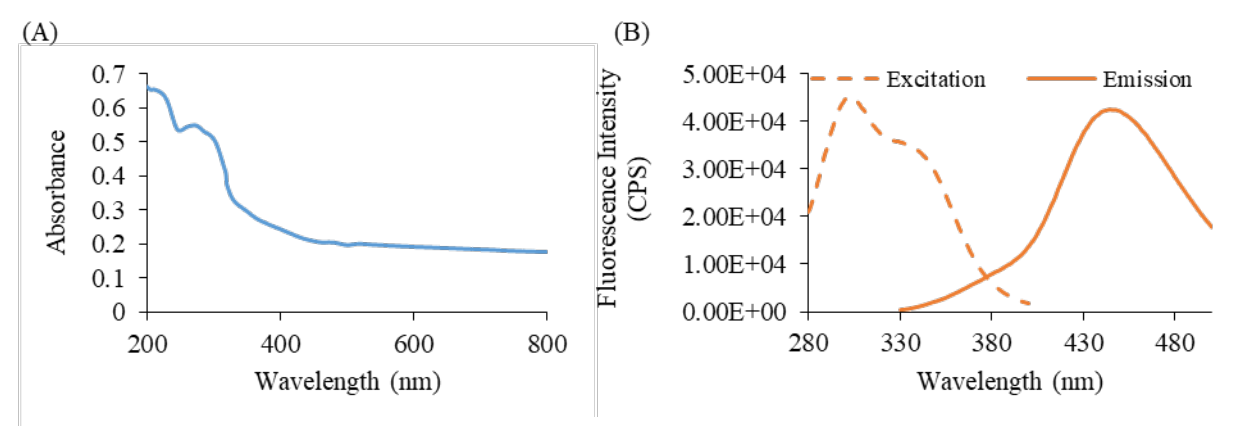


Figure 7: (A) GQDs absorption profile in water at concentration of 0.1 mg/mL. Clear absorption can be observed at $\sim 300 \text{ nm}$. (B) Fluorescence profile of the GQDs (0.2 mg/mL in water) that showed the 310 nm excitation and 440 nm emission peaks.

Then, the 3D fluorescence map was collected by changing the excitation wavelength from 280 to 500 nm for both the GQDs in pH 7.0 and the pH 7.0 blank. This observation was witnessed again in the 2D fluorescence spectra (Figure 8A) which showed two fluorescence peaks in the GQDs, centering at 440 and 850 nm. In order to prove that the fluorescence was coming from the GQDs and not from the precursor, solvent, or second order excitation, a solution of CBDA-2, water, and pH 7.0 were also collected. The GQDs showed the strong fluorescence emission at 440 and 850 nm, indicating that the prepared GQDs could be used as a strong fluorescent tag in the visible and NIR range. To further confirm the NIR peak was indeed coming from the GQDs, several concentrations of the material were prepared and analyzed. Figure 8B shows that the fluorescence intensity of the GQDs in the NIR region was proportional to concentration (25 - 3.125 µg/mL). Similar with the other reported GQDs, the prepared GQDs showed excitation-dependent fluorescence emission. As shown in Figure 8C, the visible emission peak of the GQDs shifted from 440 nm to 520 nm when the excitation wavelength was changed from 280 nm to 500 nm. The highest fluorescence emission peak (Figure 8D) also showed an excitation light dependency, shifting from 850 to 900 nm. The highest fluorescence emission peak was recorded at a 340 nm excitation light.

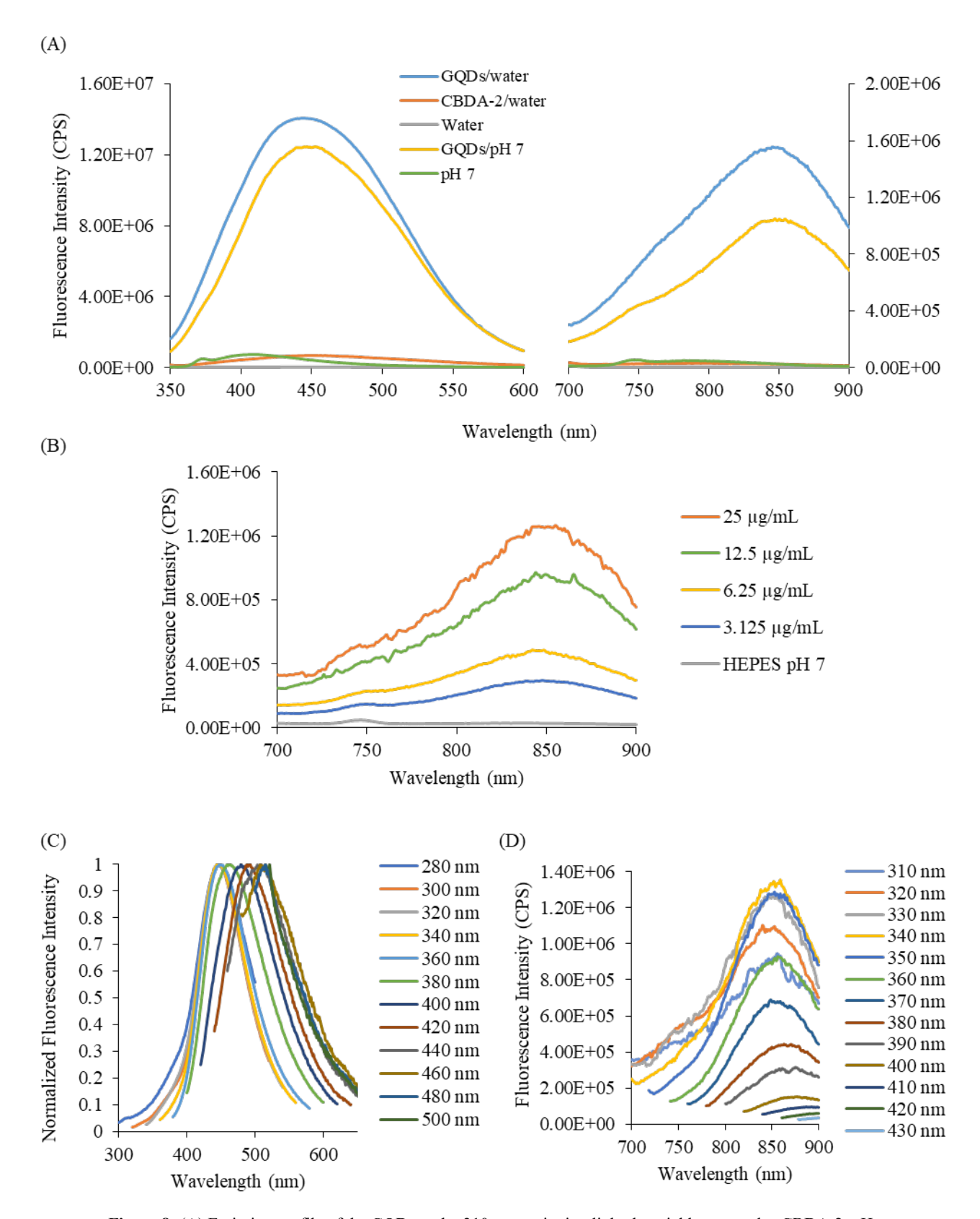


Figure 8: (A) Emission profile of the GQDs under 310 nm excitation light that yields two peaks. CBDA-2, pH 7.0, and water (solvent) were tested for interference effects. CBDA-2 and pH 7.0 showed slight emission at 440 nm but no peak was observed at 850 nm. (B) Changing concentration of GQDs NIR peak, indicating fluorescence is being emitted from the material. (C) Excitation light dependent behavior for the visible peak at 440 nm emission. (D) Excitation light dependent behavior for the NIR peak at 850 nm emission

To be utilized as a fluorescent tag in bioanalysis and bioimaging, the stability of the GQDs is critical. Therefore, the fluorescence intensity of the GQDs was studied with in different pH conditions from 1.0 to 11.0 using the HEPES buffer. The results depicted that the GQDs contained the highest fluorescence intensity in the range of pH 5-9 (Figure 9) which is ideal for biological samples. Under pH 5 or higher than pH 9, the fluorescence intensity of the GQDs decreased. Especially, the GQDs were unstable in pH 1 (maelate) where the largest quenching was observed, which might be caused by the fact that the zeta potential of the GQDs at pH 1 became almost zero, resulting in the aggregation-induced quenching of the GQDs.

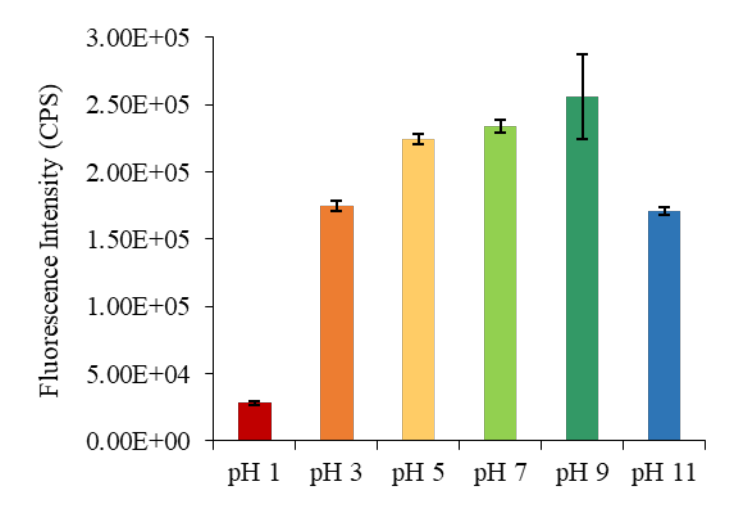


Figure 9: Fluorescence intensity measurements of the GQDs shows quenching effects in maclate pH 1.0 while pHs 3.0 - 11.0 (citrate, HEPES, CHES, and CAPS) depict relatively no significant difference in decrease or increase of intensity. All solutions were 0.2 mg/mL GQDs.

The photostability of the GQDs was analyzed with a sample of FITC being used as the standard comparison dye. The resulting data can be found in Figure 10 below. Both FITC (20 μ M) and the GQDs (80 μ g) were cultured in MCF-7 cells. Cells were incubated with GQDs for 3 hours before being fixed. After 30 min of imaging, the GQDs bleached to only 60% of their original intensity while FITC bleached to 20% in the first 300-400 seconds. This provides helping insight into the GQDs photostability and potential to be used for prolonged analyses in other applications that require it.

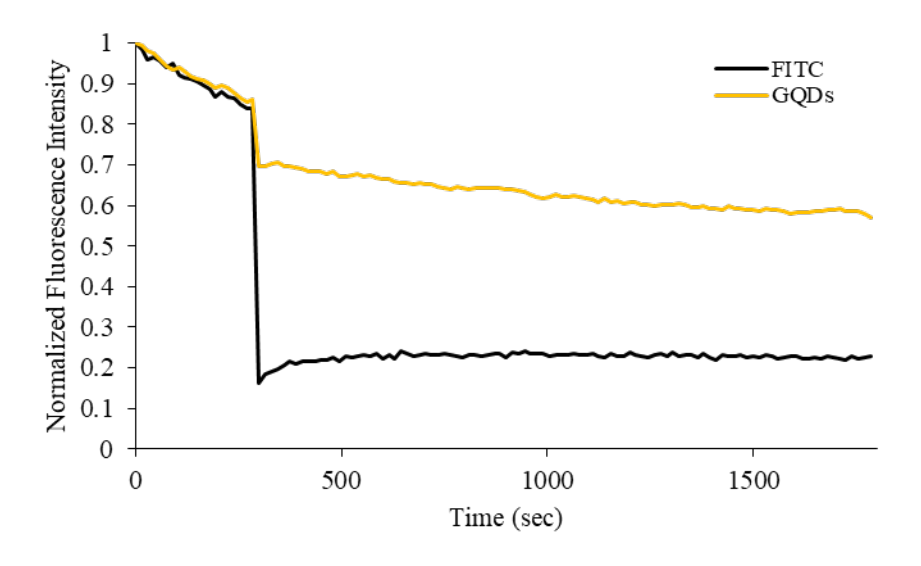


Figure 10: Photostability of the GQDs compared to FITC dye.

3.4. In vitro cell imaging with MCF-7 cells doped with GQDs

Based on the promising fluorescence properties, we tested the feasibility of the GQDs to be used as a fluorescent agent for cell staining. Before the imaging application, the cytotoxicity of the GQDS was evaluated by MTT assay in RAW 246.7 cells due to the pinocytosis property. The results showed that negatable toxicity was observed even when the concentration of the GQDs was as high as 200 µg/mL (Figure 11), indicating the superior biocompatibility of GQDs obtained from the biomass. However, GQDs have been reported to show toxic effects and a decrease in cell viability at 500 µg/mL exposures.^{66,67}

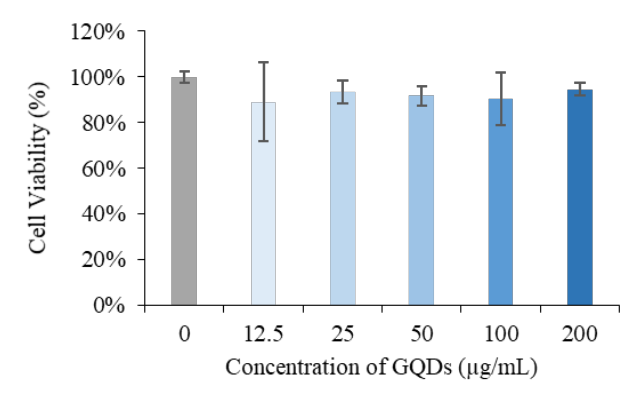


Figure 11: Cultured RAW cells with various concentrations of GQDs. The highest cell death occurs at 12.5 μ g/mL, while no culture exceeded 20% total cell death compared to the control.

MCF-7 cells were used for the GQDs confocal imaging because of the epithelial-like morphology and the formed monolayer. GQDs were incubated with the MCF-7 cells for 3 hours, the cells were fixed and imaged using a fluorescence confocal microscope. As shown in Figure 12, the MCF-7 cells incubated with the GQDs showed strong green fluorescence (Alex 488 channel) upon excitation at 405 nm, indicating that the GQDs entered the cells through endocytosis. ^{68,69} In contrast, no apparent fluorescence was observed in the green channel when the MCF-7 cells were incubated with TOPRO-3 labeled nuclei (Figure 12A). The fluorescence intensity of the cells were quantified using ImageJ software, and the results demonstrated that the fluorescence intensity of the MCF-7 cells incubated with the GQDs was three-fold higher than the pure cells, indicating that GQDs could be used as strong fluorescent tags to label both cell membranes and the cytoplasm. Incubating the GQDs with MCF-7 cells resulted in the GQDs entering the cells through endocytosis and imaged using confocal microscopy. The two colored channels and the bright-field images are depicted below (Figure 12B). It is clearly observed that when the GQDs are were added, the intensity across the channels also increased, mostly in the green channel but a slight increase was also observed for the red channel.

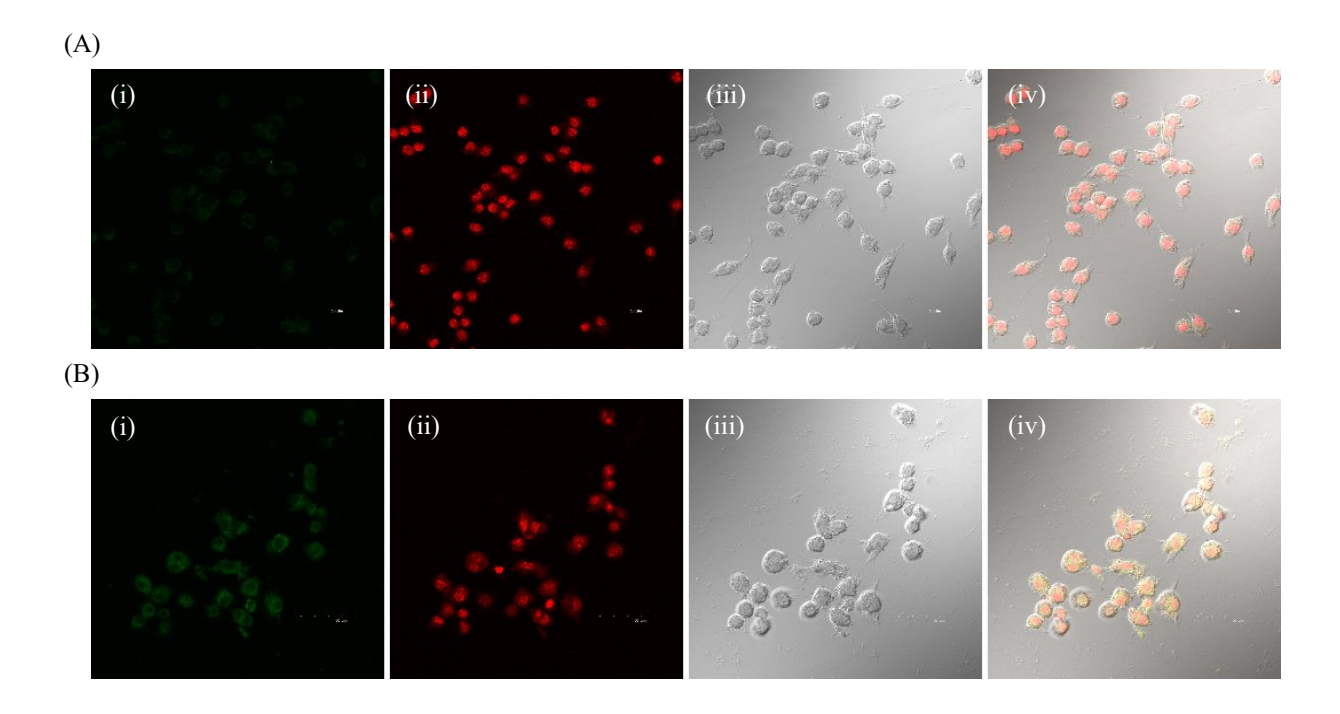


Figure 12: *In vitro* images of MCF-7 cells cultured with GQDs: (A) TOPRO-3 labeled nuclei of MCF-7 cells; (B) 100 μL of 0.8 mg/mL GQDs and MCF-7 cells. Columns are two excitation channels used as well as the microscope images: (i) Alexa 488, (ii) Fura-Red (Ca-free), (iii) Bright-field and (iv) Overlaid.

3.5. Metal ion detection using the GQDs

The fluorescence bioimaging is the main application of the developed GQDs. Additionally, the GQDs were found to be capable of metal ion detection. Thus, five common metal ions in solution: Cu^{2+} , Fe^{3+} , Fe^{2+} , Hg^{2+} , and Pb^{2+} were tested using the GQDs (Figure 13). As a result, Hg^{2+} showed the greatest quenching for a higher concentration of 100 μ M. Pb^{2+} showed little to no quenching across the concentrations and the remaining ions of Cu^{2+} , Fe^{3+} , and Fe^{2+} showed quenching at the highest concentration (100 μ M) but no significant decrease in fluorescence was observed for the 10 and 1.0 μ M solutions. Therefore, the detection of Hg^{2+} was further studied using the GQDs by optimization of experimental conditions temperature and pH.

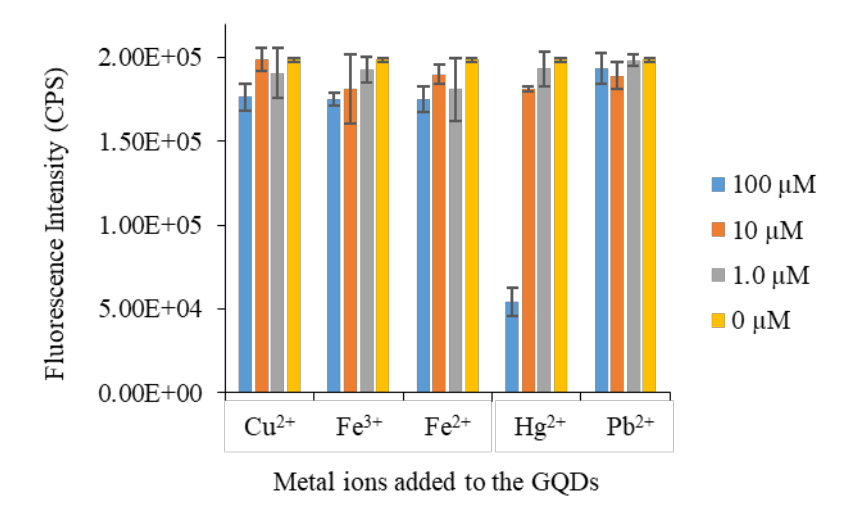


Figure 13: Metal ion detection using 0.1 mg/mL GQDs in HEPES buffer pH 7.0: Cu^{2+} , Pb^{2+} , Fe^{2+} , Fe^{3+} , and Hg^{2+} were added in 100, 10, and 1 μ M final concentrations.

For optimization, 2^4 factorial screening was first used to identify estimated parameters for optimal conditions, those being pH, temperature, concentration of Hg²⁺, and concentration of GQDs. The high and low conditions can be found in Table 1 as well as the center point conditions. After screening, a regression model was fit to the data to estimate the relationships between the dependent variables. A normality test of the residuals helped to verify the model's accuracy, yielding a p-value greater than the α -value of 0.05 which indicates that the residuals are normally distributed. Due to this, the model interference can be confirmed as validated and thus an optimization analysis on the data was performed as well.

Table 1: 2⁴ factorial screening DOE method applied to the optimization analysis of the GQDs, Hg²⁺, temperature, and pH conditions.

Factor	Low (-1)	High (+1)	Center Point (CtPt)
рН	3.0	9.0	6.0
Temperature	2 °C	50 °C	26 °C
Concentration of Hg ²⁺	1.0 μΜ	100 μΜ	50.5 μΜ
Concentration of GQDs	0.02 mg/mL	0.50 mg/mL	0.26 mg/mL

After analyzing the results, the Pareto chart of all factors and interactions (Figure 14A) shows that out of the four factors, only concentration of Hg²⁺ and concentration of GQDs were significant. Temperature had no effect as a main factor, nor did its interaction have any impact on the overall fluorescence intensity. Additionally, pH as a main factor had no direct effect, however, its interaction on both the mercury ions and GQDs was significant. Therefore, all insignificant factors and interactions were removed from the terms and the Pareto chart was plotted again (Figure 14B).

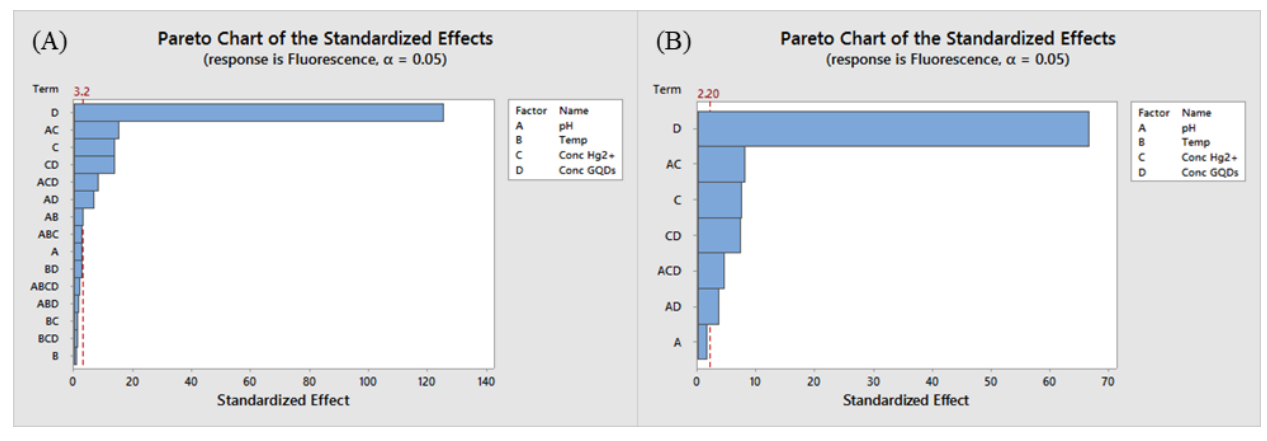


Figure 14: (A) Pareto chart of the full factorial analysis of fluorescence intensity with all interactions included. (B) Pareto chart of refined terms of the full factorial analysis after removing temperature as well as other insignificant interactions.

As previously stated, the optimization analysis was also conducted to help verify the 2⁴ design above. To confirm this, the model was set to predict the conditions that would yield the highest fluorescence intensity. The model predicted that pH 9, 0.50 mg/mL GQDs, and 1.0 μM Hg²⁺ were the most optimal conditions for the highest intensity. For convenience, the triplicate runs of the optimal conditions were conducted at room temperature (26 °C) given that the model predicted temperature to be an insignificant factor. Figure 15 depicts all sixteen factorial samples and the four center points in comparison to the optimal condition samples in gray. The triplicate runs confirmed the DOE experiment by having an equal average fluorescence intensity as sample 10 (pH 9.0, 2 °C, 1.0 μM Hg²⁺, 0.50 mg/mL GQDs) which had the highest fluorescence out of the twenty screening samples and sample 12 (pH 9.0, 50 °C, 1.0 μM Hg²⁺, 0.50 mg/mL GQDs) was second. Additionally, the optimization predictor showed that for higher concentrations of Hg²⁺, a more acidic environment yields a higher fluorescence intensity and for lower concentrations, basic conditions have higher fluorescence intensities. Furthermore, decreasing the concentration of the GQDs decreases the quenching sensitivity, as the 0.02 mg/mL samples yielded nearly the same intensity for the 100 and 1.0 μM Hg²⁺ additives, regardless of temperature and pH. However, increasing the concentration of GQDs to 0.5 mg/mL also did not drastically increase the sensitivity, with similar complications arising from the 1.0 μM detection as observed in Figure 13 with 0.2 mg/mL of GQDs.

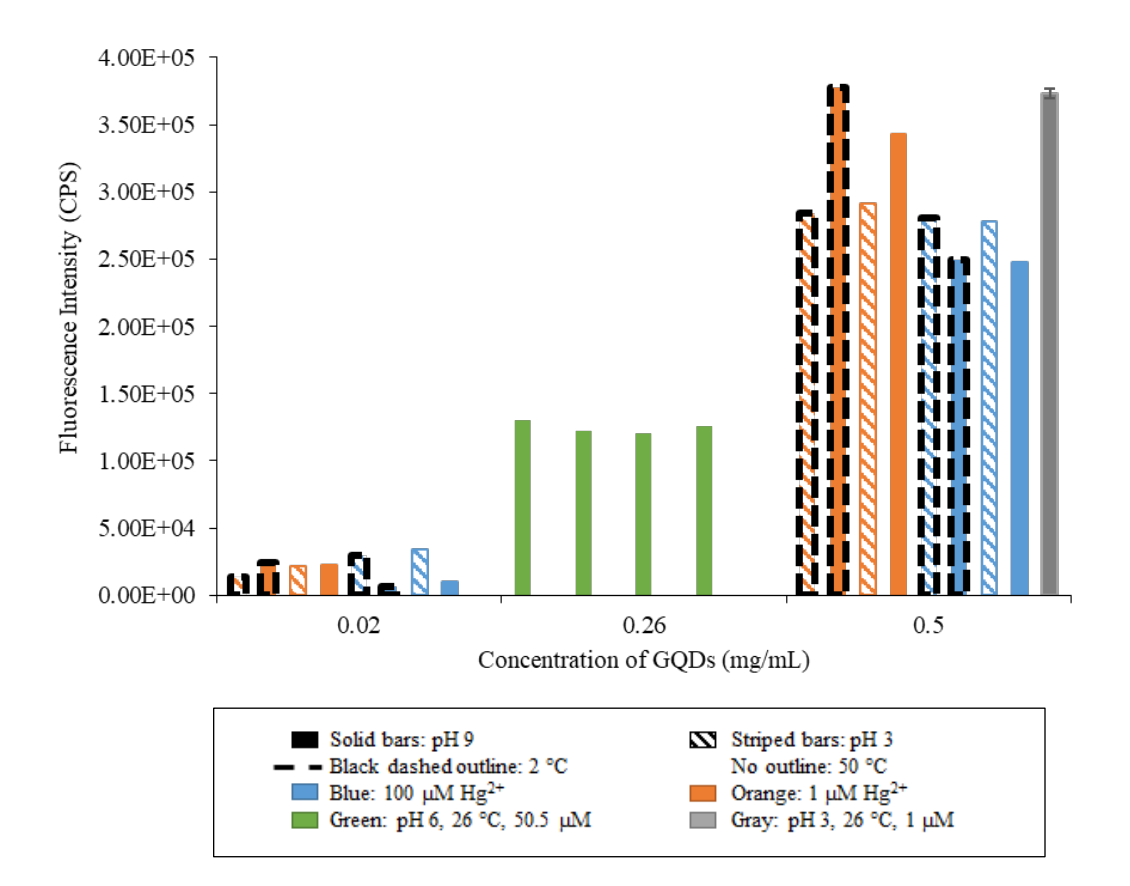


Figure 15: All sixteen samples and four center points in comparison to the optimal condition samples (gray). The optimized samples were run in triplicate and their average result contained the highest fluorescence intensity.

Additional concentrations of Hg^{2+} ions were then tested for a better detection limit analysis, ranging from 1 to 100 μ M (Figure 16). At lower concentrations, 1 and 5 μ M, not only did the standard deviation increase but the difference compared to the control was negligible. Concentrations greater than 10 μ M where better detected, with a limit of detection (LOD) of 2.5 μ M and limit of quantitation (LOQ) of 8.3 μ M.

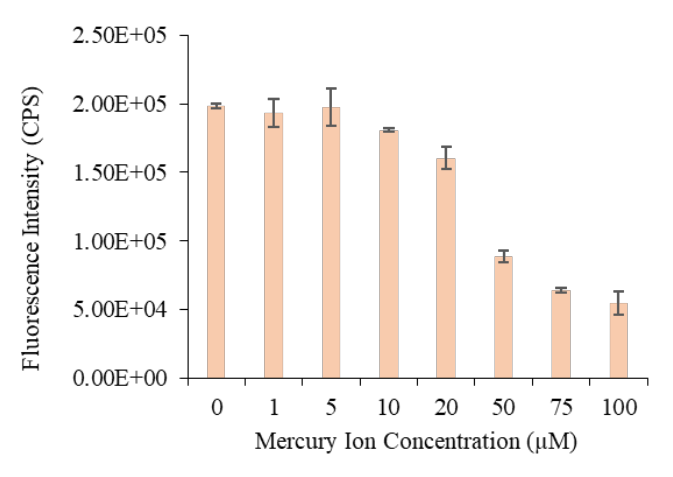


Figure 16: Mercury ion detection using the (0.2 mg/mL) GQDs at room temperature in 20 mM pH 7.0 HEPES buffer. LOD: 2.5 μ M. LOQ: 8.3 μ M.

4. Conclusion

Graphene quantum dots (GQDs) were successfully synthesized by pyrolysis of biomass-derived CBDA-2 under basic conditions. The optical properties were thoroughly investigated and the GQDs yielded two distinct emission peaks (440 and 850 nm) with one excitation wavelength (310 nm). The GQDs were also stable across a wide pH range, only showing quenching at pH 1.0 and prolonged photostability up to 30 min. When exposed to various metal ions, the GQDs were only quenched by mercury ions down to 10 μM concentrations, LOQ of 8.3 μM. The *in vitro* imaging of MCF-7 depicted strong fluorescent images of the GQDs in the Alexa 488 channel in and RAW 246.7 cells showed excellent biocompatibility. Overall, we developed strong fluorescent GQDs from biomass, providing a novel method for generating fluorescent GQDs for bioanalysis and bioimaging.

Acknowledgments

This work was supported by the NSF grant CHE 1709160 and NSF EPSCoR RII Track I Cooperative Agreement 1946202. The authors acknowledge the use of the Edward C. Carlson Imaging and Image Analysis Core Facility supported in part by NIH grant 1P30GM103329, and the use of the North Dakota INBRE Microscopy Core Facility supported in part by NIH grant P20GM103442.

References

- Wang, D.; Chen, J.; and Dai, L. Recent Advances in Graphene Quantum Dots for Fluorescence Bioimaging from Cells Through Tissues to Animals. *Part. Part. Syst. Charact.* 2015, 32, 515-523.
- 2. Gurunathan, S.; Kim, E.; Han, J.; Park, J.; and Kim, J. Green Chemistry Approach for Synthesis of Effective Anticancer Palladium Nanoparticles. *Molecules*. **2015**, *20*, 22476-22498.
- Liu, J.; Zhang, F.; Allen, A.; Johnston-Peck, A.; and Pettibone, J. Comparing Sulfidation Kinetics of Silver Nanoparticles in Simulated Media Using Direct and Indirect Measurement Methods. *Nanoscale.* 2018, 10, 22270-22279.
- 4. Griffin, S.; Masood, M.; Nasim, M.; Sarfraz, M.; Ebokaiwe, A.; Schäfer, K.; Keck. C.; and Jacob, C. Natural Nanoparticles: A Particular Matter Inspired by Nature. *Antioxidants*. **2018**, *7*, 3.
- 5. Chen, W.; Lv, G.; Hu, W.; Li, D.; Chen, S.; and Dai, Z. Synthesis and Applications of Graphene Quantum Dots: A Review. *Nanotechnol Rev.* **2018**, *7*(2), 157-185.
- 6. Tadyszak, K.; Wychowaniec, J.; and Litowczenko, J. Biomedical Applications of Graphene-based Structures.

 Nanomaterials. 2018, 8, 944-964.
- Atchudan, R.; Edison, T.; Perumal, S.; Clament Sagaya Selvam, N.; and Lee, Y. Green Synthesized Multiple
 Fluorescent Nitrogen-doped Carbon Quantum Dots as an Efficient Label-free Optical Nanoprobe for In Vivo
 Live-cell Imaging. J. Photochem Photobiol A. 2019, 372, 99-107.
- 8. Sun, J.; Cui, F.; Zhang, R.; Gao, Z.; Ji, J.; Ren, Y.; Pi, F.; Zhang, Y.; and Sun, X. Comet-like Heterodimers "Gold Nanoflower @Graphene Quantum Dots" probe with FRET "Off" to DNA Circuit Signal "On" for Sensing and Imaging MicroRNA In Vitro and In Vivo. *Anal. Chem.* **2018**, *90*, 11538-11547.
- 9. Zhao, M. Direct Synthesis of Graphene Quantum Dots with Different Fluorescence Properties by Oxidation of Graphene Oxide Using Nitric Acid. *Appl. Sci.* **2018**, *8*, 1303-1313.

- 10. Jiang, D.; Chen, Y.; Li, W.; Wang, Z.; Zhu, J.; Zhang, H.; Liu, B.; and Xu, S. Synthesis of Luminescent Graphene Quantum Dots with High Quantum Yield and Their Toxicity Study. *Plos One.* **2015**, *10(12)*.
- 11. Tian, P.; Tang, L.; Teng, K.; and Lau, S. Graphene Quantum Dots from Chemistry Applications. *Mater. Today. Chem.* **2018**, *10*, 221-258.
- 12. Şenel, B.; Demir, N.; Büyükköroğlu, G.; and Yıldız, M. Graphene Quantum Dots: Synthesis, Characterization, Cell Viability, Genotoxicity for Biomedical Applications. *Saudi Pharm. J.* **2019**.
- Ting, S.; Ee, S.; Ananthanarayanan, A.; Leong, K.; and Chen, P. Graphene Quantum dots Functionalized Gold Nanoparticles for Sensitive Electrochemical Detection of Heavy Metal Ions. *Electrochimica Acta*. 2015, 172, 7-11.
- 14. Zhou, C.; Jiang, W.; and Via, B. Facile Synthesis of Soluble Graphene Quantum Dots and its Improved Property of Detecting Heavy Metal Ions. *Colloids Suf B Biointerfaces*. **2014**, *118*, 72-76.
- Yousaf, M.; Ahmad, M.; Ahmad Bhatti, I.; Nasir, A.; Hasan, M.; Jian, X.; Kalantar-Zadeh, K.; and Mahmood,
 N. In Vivo and In Vitro Monitoring of Amyloid Aggregation via BSA@FGQDs Multimodal Probe. ACS
 Sens. 2019, 4, 200-210.
- Liu, J.; Qin, L.; Kang, S.; Li, G.; and Li, X. Gold Nanoparticles/Glycine Derivatives/Graphene Quantum Dots Composite with Tunable Fluorescence and Surface Enhanced Raman Scattering Signals for Cellular Imaging. *Mater. Design.* 2017, 123, 32-38.
- Zhao, W.; Li, Y.; Yang, S.; Chen, Y.; Zheng, J.; Liu, C.; Qing, Z.; Li, J.; and Yang, R. Target-activated Modulation of Dual-color and Two-photon Fluorescence of Graphene Quantum Dots for In Vivo Imaging of Hydrogen Peroxide. *Anal. Chem.* 2016, 88, 4833-4840.
- Nair, R.; Thomas, R.; Sankar, V.; Muhammad, H.; Dong, M.; and Pillai, S. Rapid, Acid-free Synthesis of High-Quality Graphene Quantum Dots for Aggregation Induced Sensing of Metal Ions and Bioimaging. ACS Omega. 2017, 2, 8051-8061.
- Kalluri, A.; Debnath, D.; Dharmadhikari, B.; and Patra, P. Graphene Quantum Dots: Synthesis and Applications. *Methods Enzymol.* 2018, 609, 335-353.
- 20. Zeng, X.; Yuan, Y.; Wang, T.; Wang, H.; Hu, X.; Fu, Z.; Zhang, G.; Liu, B.; and Lu, G. Targeted Imaging and Induction of Apoptosis of Drug-resistant Hepatoma Cells by miR-122-loaded Graphene-lnP Nanocompounds. *Nanobiotechnol.* **2017**, *15:9*.

- 21. Yao, C.; Tu, Y.; Ding, L.; Li, C.; Wang, J.; Fang, H.; Huang, Y.; Zhang, K.; Lu, Q.; Wu, M.; and Wang, Y. Tumor Cell-specific Nuclear Targeting of Functionalized Graphene Quantum Dots In Vivo. *Bioconjugate Chem.* 2017, 28, 2608-2619.
- Ramachandran, S.; Sathishkumar, M.; Kothurkar, N.; and Senthilkumar, R. Synthesis and Characterization of Graphene Quantum Dots/Cobalt Ferrite Nanocomposite. *IOP. Conf. Ser.:Mater. Sci. Eng.* 2018, 310 012139.
- Zhang, L.; Peng, D.; Lian, R.; and Qiu, J. Graphene-based Optical Nanosensors for Detection of Heavy Metal Ions. *Trends Anal. Chem.* 2018, 102, 280-289.
- 24. Feng, L.; Wu, Y.; Zhang, D.; Hu, X.; Zhang, J.; Wang, P.; Song, Z.; Zhang, X.; and Tan, W. Near Infrared Graphene Quantum Dots-based Two-photon Nanoprobe for Direct Bioimaging of Endogenous Ascorbic Acid in Living Cells. *Anal. Chem.* 2017, 89, 4077-4084.
- 25. Huang, D.; Zhou, H.; Wu, Y.; Wang, T.; Sun, L.; Gao, P.; Sun, Y.; Huang, H.; Zhou, G.; and Hu, J. Bottom-up Synthesis and Structural Design Strategy for Graphene Quantum Dots with Tunable Emission to the Near Infrared Region. *Carbon.* 2019, 142, 673-684.
- 26. Bao, X.; Yuan, T.; Chen, J.; Zhang, B.; Li, D.; Zhou, D.; Jing, P.; Xu, G.; Wang, Y.; Holá, K.; Shen, D.; Wu,
 C.; Song, S.; Liu, C.; Zboîil, R.; and Qu, S. In Vivo Theranostics with Near-Infrared-Emitting Carbon Dots
 Highly Efficient Photothermal Therapy Based on Passive Targeting After Intravenous Administration.
 Light Sci. Appl. 2018, 7(91).
- 27. Laurenti, M.; Paez-Perez, M.; Algarra, M.; Alonso-Cristobal, P.; Lopen-Cabarcos, E.; Mendez-Gonzalez, D.; and Rubio-Retama, J. Enhancement of the Upconversion Emission by Visible-to-Near-Infrared Fluorescent graphene quantum dots for miRNA detection. *Appl. Mater. Interfaces.* **2016**, *8*, 12644-12651.
- 28. Tang, L.; Ji, R.; Li, X.; Bai, G.; Liu, C.; Hao, J.; Lin, J.; Jiang, H.; Teng, K.; Yang, Z.; and Lau, S. Deep Ultraviolet to Near-Infrared Emission and Photoresponse in Layered N-doped Graphene Quantum Dots. *ACS Nano.* 2014, 8(6), 6312.
- 29. Ayoubi, M.; Naserzadeh, P.; Hashemi, M.; Rostami, M.; Tamjid, E.; Tavakoli, M.; and Simchi, A. Biochemical Mechanisms of Dose-dependent Cytotoxicity and ROS-mediated Apoptosis Induced by Lead Sulfide/Graphene Oxide Quantum Dots for Potential Bioimaging Applications. Sci. Reports. 2017, 7, 12896.

- 30. Lee, B.; McKinney, R.; Hasan, T.; and Naumov, A. Graphene Quantum Dots as Intracellular Imaging-based Temperature Sensors. *Materials*. **2021**, *14*, 616.
- Tayyebi, A.; Akhavan, O.; Lee, G.; and Outokesh, M. Supercritical Water in Top-down Formation of Tunable-sized Graphene Quantum Dots Applicable in Effective Photothermal Treatments of Tissues. Carbon. 2018, 130, 267-272.
- 32. Kumawat, M.; Thakur, M.; Gurung, R.; and Srivastava, R. Graphene Quantum Dots from Mangifera Indica:
 Application in Near-Infrared Bioimaging and Intracellular Nanothermometry. *ACS Sustainable Chem. Eng.* **2017**, *5*, 1382-1391.
- 33. Zhu, P.; Zhang, T.; Li, J.; Ma, J.; Ouyang, X.; Zhao, X.; Xu, M.; Wang, D.; and Xu, Q. Near-infrared Emission Cu, N-doped Carbon Dots for Human Umbilical Vein Endothelial Cell Labeling and Their Biocompatibility In Vitro. J. Appl. Toxicol. 2021, 41(5), 789-798.
- 34. Huang, P.; Shi, J.; Zhang, M.; Jiang, X.; Zhong, H.; Ding, Y.; Cao, X.; Wu, M.; and Lu, J. Anomalous Light Emission and Wide Photoluminescence Spectra in Graphene Quantum Dot: Quantum Confinement from Edge Microstructure. J. Phys. Chem. Lett. 2016, 7, 2888-2892.
- 35. Kuo, Q.; Shen, X.; Chang, C.; Kao, H.; Lin, S.; Wang, J.; and Wu, P. Multiplexed Graphene Quantum Dots with Excitation-Wavelength-Independent Photoluminescence, as Two-photon Probes, and in Ultraviolet-Near Infrared Bioimaging. ACS Nano. 2020, 14, 11502-11509.
- 36. Jeong, H.; Song, J.; Jeong, S.; and Chang, W. Graphene/PbS Quantum Dot Hybrid Structure for Application in Near-Infrared Photodetectors. *Sci. Rep.* **2020**, *10*, 12475.
- 37. Hai, X.; Feng, J.; Chen, X.; and Wang, J. Tuning the Optical Properties of Graphene Quantum Dots for Biosensing and Bioimaging. *J. Mater. Chem. B.* **2018**, *6*, 3219-3234.
- 38. Chen, F.; Gao, W.; Qui, X.; Zhang, H.; Liu, L.; Liao, P.; Fu, W.; and Luo, Y. Graphene Quantum Dots in Biomedical Applications: Recent Advances and Future Challenges. *Front. Lab. Med.* **2017**, *1*, 192-199.
- 39. Li, K.; Liu, W.; Ni, Y.; Li, D.; Lin, D.; Su, Z.; and Wei, G. Technical Synthesis and Biomedical Applications of Graphene Quantum Dots. *J. Mater. Chem. B.* **2016**, *00*, 1-3.
- 40. Wang, L.; Wang, Y.; Xu, T.; Liao, H.; Yao, C.; Liu, Y.; Li, Z.; Chen, Z.; Pan, D.; Sun, L.; and Wu, M. Gram-Scale Synthesis of Single-Crystalline Graphene Quantum Dots with Superior Optical Properties. *Nat. Commun.* 2014, 5, 5357. https://doi.org/10.1038/ncomms6357.

- 41. Tang, L.; Ji, R.; Cao, X.; Lin, J.; Jiang, H.; Li, X.; Teng, K. S.; Luk, C. M.; Zeng, S.; Hao, J.; and Lau, S.P. Deep Ultraviolet Photoluminescence of Water-Soluble Self-Passivated Graphene Quantum Dots. *ACS Nano* 2012, 6, 5102–5110. https://doi.org/10.1021/nn300760g.
- Wang, Z.; Yu, J.; Zhang, X.; Li, N.; Liu, B.; Li, Y.; Wang, Y.; Wang, W.; Li, Y.; Zhang, L.; Dissanayake, S.; Suib, S.L.; and Sun, L. Large-Scale and Controllable Synthesis of Graphene Quantum Dots from Rice Husk Biomass: A Comprehensive Utilization Strategy. ACS Appl. Mater. Interfaces. 2016, 8 (2), 1434–1439. https://doi.org/10.1021/acsami.5b10660.
- 43. Suryawanshi, A.; Biswal, M.; Mhamane, D.; Gokhale, R.; Patil, S.; Guin, D.; and Ogale, S. Large Scale Synthesis of Graphene Quantum Dots (GQDs) from Waste Biomass and Their Use as an Efficient and Selective Photoluminescence on–off–on Probe for Ag⁺ Ions. *Nanoscale* **2014**, *6* (20), 11664–11670. https://doi.org/10.1039/C4NR02494J.
- 44. Prasannan, A.; and Imae, T. One-Pot Synthesis of Fluorescent Carbon Dots from Orange Waste Peels. *Ind. Eng. Chem. Res.* **2013**, *52* (44), 15673–15678. https://doi.org/10.1021/ie402421s.
- 45. Park, S. Y.; Lee, H. U.; Park, E. S.; Lee, S. C.; Lee, J.-W.; Jeong, S. W.; Kim, C. H.; Lee, Y.-C.; Huh, Y. S.; and Lee, J. Photoluminescent Green Carbon Nanodots from Food-Waste-Derived Sources: Large-Scale Synthesis, Properties, and Biomedical Applications. ACS Appl. Mater. Interfaces 2014, 6 (5), 3365–3370. https://doi.org/10.1021/am500159p.
- 46. Dong, Y.; Shao, J.; Chen, C.; Li, H.; Wang, R.; Chi, Y.; Lin, X.; and Chen, G. Blue Luminescent Graphene Quantum Dots and Graphene Oxide Prepared by Tuning the Carbonization Degree of Citric Acid. *Carbon* N. Y. 2012, 50 (12), 4738–4743. https://doi.org/https://doi.org/10.1016/j.carbon.2012.06.002.
- 47. Wu, X.; Tian, F.; Wang, W.; Chen, J.; Wu, M.; and Zhao, J. X. Fabrication of Highly Fluorescent Graphene Quantum Dots Using L-Glutamic Acid for in Vitro/in Vivo Imaging and Sensing. *J. Mater. Chem. C* 2013, 1 (31), 4676–4684. https://doi.org/10.1039/C3TC30820K.
- 48. Ding, Z.; Li, F.; Wen, J.; Wang, X.; and Sun, R. Gram-Scale Synthesis of Single-Crystalline Graphene Quantum Dots Derived from Lignin Biomass. *Green Chem.* **2018**, *20* (6), 1383–1390. https://doi.org/10.1039/C7GC03218H.

- 49. Bozell, J. J.; and Petersen, G. R. Technology Development for the Production of Biobased Products from Biorefinery Carbohydrates—the US Department of Energy's "Top 10" Revisited. *Green Chem.* **2010**, *12* (4), 539–554. https://doi.org/10.1039/B922014C.
- Mika, L. T.; Cséfalvay, E.; and Németh, Á., Catalytic Conversion of Carbohydrates to Initial Platform
 Chemicals: Chemistry and Sustainability Chem. Rev. 2018, 118, 505-613.

 https://pubs.acs.org/doi/10.1021/acs.chemrev.7b00395.
- 51. Bender, T. A.; Dabrowski, J. A.; and Gagné, M. R. Homogeneous Catalysis for the Production of Low-volume, High-value Chemicals from Biomass *Nat. Rev. Chem.* **2018**, *2*, 35-46. https://www.nature.com/articles/s41570-018-0005-y.
- 52. Wang, Z.; Scheuring, M.; Mabin, M.; Shahni, R.; Wang, Z. D.; Ugrinov, A.; Butz, J.; and Chu, Q. R. Renewable Cyclobutane-1,3-dicarboxylic Acid (CBDA) Building Block Synthesized from Furfural via Photocyclization *ACS Sustainable Chem. Eng.* **2020**, *8*, 8909-8917. https://pubs.acs.org/doi/10.1021/acssuschemeng.0c00708.
- 53. Wang, Z. D.; Elliott, Q.; Wang, Z.; Setien, R.; Puttkammer, J.; Ugrinov, A.; Lee, J.; Webster, D.; and Chu, Q. Furfural-derived Diacid Prepared by Photoreaction for Sustainable Materials Synthesis. ACS Sustainable Chem. Eng. 2018, 6, 8136-8141. https://pubs.acs.org/doi/abs/10.1021/acssuschemeng.8b02415.
- 54. Horiba, https://www.horiba.com/en_en/applications/materials/material-research/quantum-dots/recording-fluorescence-quantum-yields/, accessed 6 December 2019.
- 55. Rode, J.E.; Dobrowolski, J.C.; and Rzączyńska, Z. DFT Conformation and IR spectra of 1,1-Dicarboxycylobutane. *J. Mol. Struct.* **2002**, *642*, 147-156.
- 56. NIST, https://webbook.nist.gov/cgi/inchi?ID=C1124136&Mask=80, accessed 1 December 2019.
- 57. Yu, N.; Peng, H.; Xiong, H.; Wu, X.; Wang, X.; Li, Y.; and Chen, Y. Graphene Quantum Dots Combined with Copper(II) Ions as a Fluorescent Probe for Turn-on Detection of Sulfide Ions. *Microchim Acta*. **2015**, 182(13-14), 2139-2146.
- 58. Fan, T.; Zeng, W.; Tang, W.; Tuan, C.; Tong, S.; Cai, K.; Liu, Y.; Huang, W.; Min, Y.; and Epstein, A.J. Controllable Size-selective Method to Prepare Graphene Quantum Dots from Graphene Oxide. *Nanoscale. Res. Lett.* **2015**, *10*, 55.

- 59. Liu, Q.; Zhang, J.; He, H.; Huang, G.; Zing, B.; Jia, J.; and Zhang, C. Green Preparation of High Yield Fluorescent Graphene Quantum Dots from Coal-Tar-Pitch by Mild Oxidation. *Nanomaterials*. **2018**, *8*(10), 844.
- 60. Vasimalai, N.; Vilas-Boas, V.; Gallo, J.; de Fátima Cerqueira, M.; Ménendez-Miranda, M.; Costa-Fernández, J.; Diéguez, L.; Espiña, B.; and Fernández-Argüelles, T. Green synthesis of fluorescent carbon dots from species for in vitro imaging and tumour cell growth inhibition. *Beilstein J. Nanotechnol.* 2018, 9, 530-544.
- Chhabra, V.A.; Kaur, R.; Kumar, N.; Deep, A.; Rajesh, C.; and Kim, K. Synthesis and Spectroscopic Studies
 of Functionalized Graphene Quantum Dots with Diverse Fluorescence Characteristics. *RSC Adv.* 2018, 8,
 11446-11454.
- 62. Moulder, J.; Stickle, W.; Sobol, P.; and Bomben, K. *Handbook of X-ray Photoelectron Spectroscopy*. Perkin-Elmer Corporation: Eden Prairie, 1992, 40-44.
- 63. Hashemzadeh, N.; Hasanzadeh, M.; Shadjou, N.; Eivazi-Ziaei, J.; Khoubnasabjafari, M.; and Jouyban, A. Graphene Quantum Dot Modified Glassy Carbon Electrode for Determination of Doxorubicin Hydrochloride in Human Plasma. *J. Pharm. Anal.* **2016**, *6*, 235-241.
- 64. Yan, R.; Wu, H.; Zheng, Q.; Wang, J.; Juang, J.; Ding, K.; Guo, Q.; and Wang, J. Graphene Quantum Dots Cut from the Graphene Flakes: High Electrocatalytic Activity for Oxygen Reduction and Low Cytotoxicity. *RSC Adv.* **2014**, *4*, 23097.
- Nair, R.; Thomas, R.; Sankar, V.; Muhammad, H.; Dong, M.; and Pillai, S. Rapid, Acid-free Synthesis of High-quality Graphene Quantum Dots for Aggregation Induced Sensing of Metal Ions and Bioimaging. ACS Omega. 2017, 2, 8051-8061.
- 66. Lei, Q.; Pan, T.; Ou, L.; Ye, Z.; Yu, C.; Bao, B.; Wu, Z.; Cao, D.; and Dai, L. Biocompatible Nucleus-targeted Graphene Quantum Dots for Selective Killing of Cancer Cells via DNA Damage. *Commun. Biol.* **2021**, *4*, 214.
- 67. Perini, G.; Palmieri, V.; Ciasca. G.; De Spirito, M.; and Papi, M. Unravelling the Potential of Graphene Quantum Dots in Biomedicine and Neuroscience. *Int. J. Mol. Sci.* **2020**, *21*, 3712.
- 68. Kumawat, M.; Thakur, M.; Gurung, R.; and Srvastava, R. Graphene Quantum Dots for Cell Proliferation, Nucleus Imaging, and Photoluminescent Sensing Applications. *Sci. Rep.* **2017**, *7*, 15858.

69. Oh, N.; and Park, J. Endocytosis and Exocytosis of Nanoparticles in Mammalian Cells. *Int. J. Nanomed.* **2014**, *9*, 51-63.

Table of Contents

Abstract	1
Introduction	2
Experimental	4
Materials	4
Sample solution preparation	4
Instrumentation for the characterized of GQDs	5
Synthesis of GQDs	5
Quantum yield measurement	6
Results and Discussion	6
Design of the synthesis of GQDs using biomass	6
Characterization of the synthesized GQDs	7
Optical properties of the GQDs	. 11
In vitro cell imaging with MCF-7 cells doped with GQDs	. 15
Metal ion detection using the GQDs	. 17
Conclusion	. 20
References	21